

Title:

***In vivo* modelling of chemo-resistant neuroblastoma provides new insights into chemo-refractory disease and metastasis.**

Authors:

Orli Yogev¹, Gilberto S. Almeida^{1,2}, Karen T. Barker¹, Sally L. George¹, Colin Kwok¹, James Campbell³, Magdalena Zarowiecki^{1,3}, Dimitrios Kleftogiannis⁵, Laura M. Smith¹, Albert Hallsworth¹, Philip Berry⁴, Till Möcklinghoff⁴, Hannah T. Webber¹, Laura S. Danielson¹, Bliss Buttery¹, Elizabeth A Calton¹, Barbara M. da Costa¹, Yann Jamin², Stefano Lise⁵, Gareth J. Veal⁴, Neil Sebire⁶, Simon P. Robinson², John Anderson⁷ and Louis Chesler^{1*}

Affiliations:

¹Division of Clinical Studies, The Institute of Cancer Research, London, SW7 3RP, UK

²Division of Radiotherapy and Imaging, The Institute of Cancer Research, London, SW7 3RP, UK

³CRUK-center Informatics Facility, The Institute of Cancer Research, London, SM2 5NG, UK

⁴Northern Institute for Cancer Research, Newcastle University, Newcastle upon Tyne. NE2 4HH

⁵ Centre for Evolution and Cancer, The Institute of Cancer Research, London, SM2 5NG, UK

⁶Paediatric and Development Pathology, Institute of Child Health, University College London, London, WC1N 3EH.

⁷ Cancer Section, UCL Great Ormond Street Institute of Child Health, London WC1N 1EH.

* Corresponding author: Louis Chesler

Running title: Modelling chemoresistance and metastasis in neuroblastoma

Keyword:

Neuroblastoma, mouse modeling, cyclophosphamide resistance, JAK-STAT3

Grant Support - This study was supported by grants from The Neuroblastoma Society (NES004); Children with Cancer UK (16-215) (O.Y), Cancer Research UK and EPSRC to the Cancer Imaging

Centre at ICR and RMH, in association with the MRC and Department of Health (England) (C1060/A10334 & C1060/A16464), The Wellcome Trust (091763Z/10/Z), an EPSRC Platform Grant (EP/H046526/1), NHS funding to the NIHR Biomedical Research Centre at The Royal Marsden and the ICR (G.S.A, Y.J, S.R). Cancer Research UK Programme (C18339), EU FP7, IMI2 (11064) (K.T.B). Christopher's Smile Clinical Fellowship; NIHR Biomedical Research Centre (NHR155X) (S.L.G). The Brain Tumor Charity, INSTINCT, (16-193) (L.M.S). The Felix White Cancer Charity (A.H). Cancer Research UK Programme (C18339) (C.K). Children with Cancer UK (16-218) (M.Z). Royal Marsden Children's Department Fund (H.T.W). The Neuroblastoma Society (NES003), (L.S.D). ICR HEFCE; Cancer Research UK Programme (C18339) (L.C) GOSH NIHR BRC and NIHR SI award (N.S). The Wellcome Trust (105104/Z/14/Z) (D.K, S.L). Children with Cancer UK Research Fellowship (Y.J.). CRUK, ECMC (P.B, T.M, G.J.V). CRUK C2739/A22897 (J.C), GOSHCC leadership award and GOSH NIHR Biomedical Research Centre (JA). CWCUK 16-033 (E.A.C).

Corresponding author – Professor Louis Chesler, Pediatric Cancer Biology, The Institute of Cancer Research. 15 Cotswold Road, Sutton, Surrey, SM2 5NG. Tel: +44 (0)20 8722 4035.
Louis.chesler@icr.ac.uk

Conflict of interest - The authors declare no potential conflicts of interest

Word count - 4862, Figures- 6, Tables- 2
Supplementary materials - Figures- 6, Tables- 6, File- 1

ABSTRACT:

Neuroblastoma is a pediatric cancer that is frequently metastatic and resistant to conventional treatment. In-part, a lack of natively metastatic, chemoresistant *in vivo* models has limited our insight into the development of aggressive disease. The Th-*MYCN* genetically-engineered mouse model develops rapidly-progressive chemosensitive neuroblastoma and lacks clinically-relevant metastases. To study tumor progression in a context more reflective of clinical therapy, we delivered multi-cycle treatment with cyclophosphamide to Th-*MYCN* mice, individualizing therapy using MRI, to generate the Th-*MYCN*^{CPM32} model. Mice developed chemoresistance and spontaneous bone-marrow metastases. Tumors exhibited an altered immune microenvironment with increased stroma and tumor-associated fibroblasts. Analysis of copy number aberrations (CNAs) revealed genomic changes characteristic of human *MYCN*-amplified neuroblastoma, specifically copy number gains at mouse chromosome 11, syntenic with gains on human chromosome 17q. RNA sequencing revealed enriched expression of genes associated with 17q gain and upregulation of genes associated with high-risk neuroblastoma, such as the cell-cycle regulator Cyclin B1-interacting protein 1 (*Ccnblip1*) and Thymidine Kinase (*TK1*). The anti-apoptotic, pro-metastatic JAK-STAT3 pathway was activated in chemoresistant tumors, and treatment with the JAK1/JAK2 inhibitor CYT387 reduced progression of chemoresistant tumors and increased survival. Our results highlight that under treatment conditions which mimic chemotherapy in human patients, Th-*MYCN* mice develop genomic, microenvironmental and clinical features reminiscent of human chemorefractory disease. The Th-*MYCN*^{CPM32} model therefore is a useful tool to dissect in detail mechanisms that drive metastasis and chemoresistance, and highlights dysregulation of signaling pathways such as JAK-STAT3 that could be targeted to improve treatment of aggressive disease.

INTRODUCTION

Neuroblastoma is an aggressive tumor of neural crest origin. At time of diagnosis, approximately half of patients have high-risk disease defined by the presence of metastatic disease, amplification of the *MYCN* oncogene or other clinical risk criteria. Conventional multimodal treatment is intensive and is characterized by frequent development of chemoresistant, metastatic disease (1,2), reinforcing the need to develop mechanistically-targeted treatments for chemorefractory patients.

In neuroblastoma, chemoresistance relating to increased drug efflux via MDR1 and MRP transport for MRP/MDR drug-substrates, and temozolomide resistance related to upregulation of MGMT activity is well-characterized (3,4). Evidence for intra-tumoral clonal selection as a consequence of conventional treatment is emerging from sequencing of paired diagnostic:relapse tissue biopsies, where evolution of new mutations not present at diagnosis, and clonal enrichment of alterations in a limited number of genes such as *HRAS*, *BRAF* and *ALK* is described (5-7). Finally, the recent identification of two transcriptionally defined cell identity states in neuroblastoma, a “noradrenergic” state and a “mesenchymal” state, associated with increased cell motility and acquisition of chemoresistance following therapy, provides a possible framework to explain the origin of metastatic and chemorefractory disease in neuroblastoma patients (8,9). However, there are only few robust preclinical models that allow the emergence of chemorefractory metastatic disease to be monitored and mechanistically probed in detail.

To study disease evolution and progression in a context more reflective of clinical therapy, we used the well-characterized Th-*MYCN* genetically engineered mouse (GEM), which replicates many clinical and genomic features of high-risk, *MYCN*-driven neuroblastoma, with the exception of clinically evident metastases or treatment resistance typical of human patients (10,11). We asked whether any clinically relevant changes would occur in tumor behavior, microenvironmental structure, or genomic integrity in these mice, under conditions of maintained genomic stress characteristic of patients undergoing repeated cycles of chemotherapy. We administered multiple cycles of cyclophosphamide (CPM), a front-line chemotherapy drug and mainstay of neuroblastoma induction therapy, to Th-*MYCN* mice using MRI to guide dose administration and to limit tumor progression. Under these conditions, the majority of mice became refractory to CPM treatment, and developed native bone-marrow metastases characteristic of human disease. Primary tumors developed cell-intrinsic cross-resistance to additional chemotherapeutics including

vincristine and doxorubicin, and exhibited structural and microenvironmental changes, including increased collagen deposition and recruitment of tumor-associated fibroblasts. At a molecular level, we identified enhanced expression of genes associated with high risk neuroblastoma, and changes in expression of key signaling pathways such as JAK-STAT3, activation of which correlates with increased motility, invasion and cell proliferation, and advanced neuroblastoma disease progression (12,13). Using the clinical JAK1/JAK2 oral inhibitor CYT387, currently in phase 3 clinical trials in adult cancer (NCT02101021), we show that cell lines derived from CPM resistant tumors are sensitive to JAK1/2 inhibition and that *in vivo* treatment with CYT387 and CPM significantly improved survival of Th-*MYCN* mice bearing CPM resistant tumors. Taken together, these data describe a preclinical model system and approach that is useful to model the microenvironmental and molecular alterations associated with the development of invasive, treatment resistant neuroblastoma, and highlight an approach to identify potentially targetable alterations in signaling pathways such as JAK-STAT3 that may be useful to combat chemoresistance in neuroblastoma.

MATERIALS AND METHODS

Study Design

All experimental protocols were approved and monitored by The Institute of Cancer Research Animal Welfare and Ethical Review Body (PPL 70/7945, later PPL P91E52C32), in compliance with the UK Home Office Animals (Scientific Procedures) Act 1986, the United Kingdom National Cancer Research Institute guidelines for the welfare of animals in cancer research(14), and the ARRIVE guidelines (15). Th-*MYCN* mice (129X1/SvJ-Tg(Th-*MYCN*)41Waw/Nci) have been described previously (11). In this study, we used homozygous Th-*MYCN* mice in which we observe 100% tumor penetrance with mean onset of tumors at 35 ± 7.5 days, consistent with other published studies (11,16). Two to five mice were caged together and were allowed access to sterilized food and water *ad libitum*.

In vivo treatment regimen

Experimental sample size: A personal dose escalation protocol was developed aiming to achieve tumors resistant to 32 mg/kg cyclophosphamide. We enrolled animals in three steps a) to identify the dose schedule ($n = 15$), b) to test the individualized protocol ($n = 9$) and c) to incorporate imaging into the resistance protocol ($n = 9$), alongside 6 untreated animals serving as controls. Th-*MYCN* tumor-bearing mice were enrolled on trial when a trained technician detected a palpable tumor size of approximately 5 mm. Dosing was initiated with a single dose of 16 mg/kg. Tumor response was detected with palpation. Upon regrowth (following regression in size), the tumor was dosed again with 16 mg/kg. This treatment was repeated until tumors no longer responded to the dose, at which time, the dose was increased by 50%. Studies were terminated when the tumor became resistant to 32 mg/kg CPM and continued to grow to a palpable size of 15 mm or immediately upon showing any signs of ill health. Tumor size, animal weight, and overall animal well-being were scored daily throughout the study. No outliers were excluded.

In vivo tumor allografts

Wild-type littermates from the Th-*MYCN* colony were used for allograft studies. Briefly, allograft studies were repeated twice with $n = 8$ mice each experiment ($n = 4$ controls and $n = 4$ treated). Mice were injected subcutaneously unilaterally or bilaterally with 2×10^6 primary uncultured cells. Calipers were used to measure tumor diameter on two orthogonal axes 2-3 times per week. Volume was calculated using the equation; $v = 4/3\pi r^3$ (where r = radius, calculated as an average of the two axes). Dosing occurred at predetermined tumor size of 5-10 mm. Studies were terminated when the mean diameter of the tumor reached 15mm.

In vivo imaging

^1H MRI was performed on a 7T horizontal bore microimaging system (Bruker Instruments, Ettlingen, Germany) using a 3 cm birdcage volume coil. Mice were scanned at baseline and pre and post dose escalation until a final scan pre and post a last 32 mg/kg CPM dose. Anesthesia was induced by intraperitoneal injection of fentanyl citrate (0.315 mg/ml) plus fluanisone (10 mg/ml) (Hypnorm, Janssen Pharmaceutical, Oxford, England), midazolam (5 mg/ml; Hypnovel; Roche, Welwyn Garden City, England) and water (1:1:2). Core body temperature was maintained by warm air blown through the magnet bore. Anatomical T_2 -weighted coronal images were acquired through the mouse abdomen, from which tumor volumes were determined using segmentation

from regions of interest (ROI) drawn on each tumor-containing slice using in-house software (ImageView, working under IDL, ITT, Boulder, Colorado, USA).

Drugs

The following compounds were used for *in vitro* and *in vivo* experiments: Cyclophosphamide (PHR1404 Sigma-Aldrich), Momelotinib (CYT387) (S2219, Selleckchem), Vincristine (S1241, Selleckchem), Doxorubicin (S1208, Selleckchem), 4-hydroperoxy Cyclophosphamide (39800-16-30, Caymanchem).

RESULTS

Th-MYCN mice develop CPM resistance following individualized multicycle treatment

In order to identify mechanisms associated with the development of chemoresistance in neuroblastoma, we developed an individualized and MRI-guided dose escalation schedule for cyclophosphamide (CPM) treatment using the homozygous Th-MYCN model, in which 100% of homozygotes develop tumors with a mean onset of 35 ± 7.5 days. To establish the dose range and degree of sensitivity of spontaneously arising Th-MYCN tumors to CPM, we monitored dose-response via anatomical MRI and palpation. We tested initial single doses of 16 vs 32 mg/kg CPM. We found that following the 16 mg/kg dose tumors exhibited an initial partial response (PR, 40% volumetric response, RECIST), at day 2 and progressive disease (PD) at day 7, while treatment with 32 mg/kg led to a very good partial response, (VGPR, 90% volumetric response, RECIST) for up to 7 days (Figure 1 A). Treatment with 16 mg/kg CPM induced cell death, evident as increased pyknotic nuclei on histologic staining (Supplementary Figure 1 A).

In order to maximize the potential for development of resistance, we dose-adjusted and individualized treatment to maintain stable disease (SD) using CPM doses of 16-32 mg/kg for up to 120 days, (Figure 1 B-D), rendering all initially chemosensitive tumors resistant to 32 mg/kg CPM at study end (last dose, Figure 1 E). After cessation of therapy, chemoresistant tumors were rapidly progressive (4 days vs. 8 days to regrowth of initial tumor volume) (Figure 1 F), with a high Ki-67 staining index (Supplementary Figure 1 B). Resistance to 32 mg/kg CPM was induced within 5-18 dose cycles, over 34-120 days (Th-MYCN^{CPM32}) (Figure 1 G, Table 1). CPM is activated from an inactive prodrug to the cytotoxic metabolite (phosphoramidate mustard), via one or more forms of aldehyde dehydrogenases (ALDH) (17,18). To rule out altered intra-tumoral cyclophosphamide metabolism or distribution as a potential explanation for these findings, we measured intra-tumoral CPM and levels of the key metabolites 2-dechloroethyl cyclophosphamide, carboxyphosphamide and 4-Ketocyclophosphamide at 1 hour post treatment in treatment-naïve and resistant tumors, finding no significant differences in these measurements (Supplementary Figure 1 C, D). Taken together, these data indicate that multicycle exposure to cyclophosphamide treatment induces chemoresistance in this model, via mechanisms not related to altered drug penetration or modulation of canonical detoxification pathways.

Altered tumor microenvironment accompanies the development of chemoresistance

Stromal content and microenvironmental structure are biological factors that correlate with clinical aggressiveness of **human** neuroblastoma. At diagnosis, low stromal content, a high Mitosis-Karyorrhexis Index (MKI) and undifferentiated tumor morphology correlate with poor prognosis and aggressive disease. Epithelial to mesenchymal transition (EMT) is thought to accompany acquisition of a migratory/metastatic phenotype and chemoresistance (19-22). In chemoresistant mice, we observed alterations in stromal structure and extracellular matrix (ECM) content, with collagen enrichment and a 2.5-fold increase in total aggregated collagen bundles as detected by picrosirius red staining (Figure 2 A, B). Immunohistochemical analysis identified increased expression of collagen IV (Figure 2 C), and to a lesser extent collagen I and fibronectin, in CPM resistant tumors (Supplementary Figure 2 A). Furthermore, immunofluorescence analysis indicated an increase in cell-associated smooth muscle actin staining, a marker consistent with presence of cancer associated fibroblasts (Figure 2 D). Concomitant with these ECM changes, we observed coexpression of vimentin with the neural marker Tuj1 in a subpopulation of TH-*MYCN*^{CPM32} tumor cells (lower panel arrows Figure 2 E), whereas in TH-*MYCN* mice the mesenchymal marker vimentin was observed only in endothelial cells (upper arrows). These results indicate that together with the development of chemoresistance following treatment, tumors exhibit evidence of microenvironmental changes and enrichment in a subpopulation of tumor cells with mesenchymal characteristics, changes associated with EMT.

Acquisition of chemoresistance is associated with the development of tumor metastasis

Given that EMT is one mechanism by which highly motile and invasive cells are generated (23,24), we examined bone marrow in the Th-*MYCN*^{CPM32} model for presence of metastases. Tumor cells in bone marrow were identified by FACS as live, single cells, CD45 negative, CD11b negative, and GD2 (neuroblastoma antigen) positive (Figure 3 A). We found that six out of nine (66%) mice with resistant tumors had detectable tumor cells in bone marrow compared to two out of six (33%) from mice with treatment naïve tumors (Figure 3 B). Next, we used immunohistochemistry with the neural marker neurofilament-light (NF-L) to detect metastatic cells present in tibial sections. We identified multi-focal bone marrow metastases defined by positive NF-L staining in 9 of 13 (69%) Th-*MYCN*^{CPM32} mice and 0 of 6 untreated controls (Table 1 and Figure 3 C). Furthermore,

pathological examination of the metastatic foci indicated a morphological resemblance between human and murine neuroblastoma bone marrow (stained with the clinical human neuroblastoma marker CD56 and the equivalent murine marker NF-L, respectively, Figure 3 C). One intriguing interpretation of this data is that treatment and acquisition of chemoresistance in these tumors is associated with EMT in a subset of cells that migrate to bone marrow and generate disseminated metastases. This would be an obvious focus for further work in the model.

Resistant Th-MYCN^{CPM32} tumors acquire genomic changes reflective of human neuroblastoma

To identify candidate genes and pathways that are altered in resistant tumors, and which could represent potential therapeutic targets, we performed bulk gene expression analysis of treatment-naïve and resistant tumors (Supplementary Tables 1-4). We found that expression of only a small subset of genes (n = 22) was significantly altered (p < 0.05) in resistant as compared to treatment-naïve tumors (Figure 4 A). Among the upregulated genes we identified the cell cycle regulator Cyclin B1 interacting protein 1 (*Ccnblip1*), and Thymidine kinase (*TK1*), a biomarker for aggressiveness in many types of cancer (25,26). We confirmed these findings in an independent sample set using quantitative real time PCR (Figure 4 B, C). High expression levels of both genes are significantly associated with poor survival in human neuroblastoma (Figure 4 D, E) (<https://r2.amc.nl>). However, the upregulation of *TK1* was not observed at the protein level (Supplementary Figure 2 B) and quantitation of CCNB1IP1 protein was not possible due to lack of reliable antibody. To identify pathways associated with resistance in the Th-MYCN^{CPM32} model we performed gene set enrichment analysis (GSEA), identifying upregulated expression of genes associated with gain of human chromosome 17q (Figure 4 F); which, together with loss of chromosome 1p36, defines an extremely poor prognosis group in neuroblastoma with a 15.6% 5-year relapse-free survival (27).

We performed copy number (CN) analysis on whole-exome sequencing, comparing tissue obtained from sensitive tumors to resistant tumors with matched bone marrow metastases (Figure 4 G, Supplementary Figure 3 A). In 6 of 7 (85%) of resistant tumors and in 4 of 7 (57%) matched bone marrow metastases, we found gains on mouse chromosome 11 in a region spanning 100 Mbp to 120 Mbp. This locus is syntenic with human 17q gain (Supplementary Figure 3 B, Supplementary Table 5). No corresponding changes were evident in treatment naïve tumors.

Although gains on chromosome 11 have been reported in 40% of hemizygous Th-*MYCN* tumors with long latency (11), they have not previously been identified in homozygous Th-*MYCN* tumors. Three genes on the gained region (TBX4, TK1 and Tnrc6c) were within a set of 22 genes with up-regulated RNA expression in the Th-*MYCN*^{CPM32} tumors (Figure 4A). Levels of TNRC6 protein were increased in resistant tumors (Supplementary Figure 2 B). We were unable to quantitate TBX4 protein due to lack of a reliable antibody. We next evaluated tumor samples for somatic variants in genes frequently mutated in relapsed neuroblastoma; Alk, Atrx, Arid1a, Arid1b, PHOX2B, Ptpn11, Kras, Nras, Hras1 (28). Based on our sequencing coverage, in which ~97.4% of exonic positions have at least five reads and ~70.4% of exonic positions have at least 50 reads (Supplementary Table 6), no mutations in these genes were identified. These results indicate that following prolonged treatment with CPM, tumors in the Th-*MYCN* murine model exhibit one of the commonest segmental chromosomal abnormalities associated with high-risk neuroblastoma. We do not observe an accumulation of SNVs that are described as enriched in human patients at time of relapse, at least within the treatment conditions used here.

*Resistant Th-*MYCN*^{CPM32} tumors develop JAK-STAT pathway activation and other features typical of aggressive human neuroblastoma.*

One potential use of this model is to highlight altered expression of pathways that may contribute to development of chemoresistance and metastasis. Consistent with other assays suggestive of EMT in these tumors, GSEA detected upregulation of genes within the mesenchymal core-regulatory state and relative under-expression of genes associated with the adrenergic state (Supplementary Figure 3 C-E) (9).

To further explore this, we examined protein levels of the canonical adrenergic marker PHOX2B and the mesenchymal marker vimentin (9), by immunohistochemistry in tumor sections derived from the Th-*MYCN* and the Th-*MYCN*^{CPM32} mice (Supplementary Figure 4 A). Consistent with the detection of vimentin-positive neuroblastoma cells in the resistant tumors shown in Figure 2 E, we found a greater proportion of cells that were PHOX2B negative and an increase in vimentin positive cells in Th-*MYCN*^{CPM32} compared to Th-*MYCN* tumors (supplementary Figure 4 B). We next evaluated the mesenchymal status of cell lines derived from Th-*MYCN*^{CPM32} tumors. We established a panel of cell lines from a Th-*MYCN*^{CPM32} tumor derived either by directly culturing

the primary tumor *in vitro* (68557), or by passaging it *in vivo* as subcutaneous tumor (83984) or as an intratibial tumor (96459) prior to subsequent *in vitro* culture. From the intratibial tumor two cell lines were generated; 96459A and 96459B (Supplementary Figure 4 C, D). Via immunoblot, all Th-*MYCN*^{CPM32} cell lines showed a reduction in levels of the adrenergic marker PHOX2B and an increase in the levels of the mesenchymal markers vimentin and FMO3, compared to untreated Th-*MYCN* tumors and the human neuroblastoma cell lines IMR5 and KELLY (Supplementary Figure 4 E). Gene expression in these cell lines mapped very closely to established core mesenchymal, but not adrenergic, gene signatures (8,9) (Supplementary Figure 4 F). Of interest, we found reduced or negligible levels of MYCN protein (68557, 83984 and 96459B) and a reduction in *MYCN* mRNA levels (83984 and 96459B) (Supplementary Figure 4 D, G). Taken together, these results suggest that a transition to a mesenchymal state occurs in Th-*MYCN*^{CPM32} tumors following treatment.

In order to identify aberrantly regulated and potentially druggable events, we further used GSEA to investigate alterations in gene expression within these samples. We identified 15 significantly enriched KEGG pathways (Table 2) and focused on the anti-apoptotic and pro-metastatic IL6-JAK-STAT3 signaling pathway (Figure 4 H-J). We therefore compared levels of total STAT3 and activated p-STAT3 (Y705) in sensitive and resistant tumors. We found a significant enhancement of total STAT3 nuclear staining in resistant tumors compared with treatment naïve tumors (Figure 4 K, Supplementary Figure 5 A). The majority (6 of 8) of primary tumors from mice with detectable bone marrow metastases exhibited p-STAT3 staining (Table 1, Figure 4 L), as is observed in human neuroblastoma (13). Given that JAK-STAT3 pathway activation is present in these mice and is a feature associated with high-risk neuroblastoma (29), we investigated whether JAK-STAT3 pathway inhibition would alter disease progression in Th-*MYCN*^{CPM32} mice with treatment resistant tumors.

Inhibition of the JAK-STAT3 pathway leads to cytostatic cell cycle arrest

We used the clinical candidate JAK1/JAK2 ATP-competitive inhibitor CYT387 to assess efficacy of JAK STAT3 pathway inhibition. While several other JAK inhibitors are available, CYT387 is currently being used in a phase 3 randomized clinical trial for metastatic pancreatic ductal adenocarcinoma (NCT02101021). Its efficacy in neuroblastoma has not yet been tested. We tested

sensitivity to CYT387 in our Th-*MYCN*^{CPM32} tumor-derived cell line panel (68557, 83984 and 96459B, Supplementary Figure 4 C), in addition to the well-characterized human neuroblastoma cell lines, BE2C and SK-N-AS (30,31), derived from heavily pretreated patients, IMR5 (32,33), derived from a patient at time of diagnosis, and KELLY cells (treatment status unknown). To test the efficacy of CYT387 we assayed levels of p-STAT3, an indicator of JAK1/2 inhibition and of c-Fos, a known transcriptional target of STAT3 (34). Cytotoxicity was evident at 0.37 μ M (Supplementary fig 5 B) and dose-dependent inhibition of STAT3 phosphorylation on immunoblots was consistent with on-target activity (range 1 μ M - 3 μ M, Figure 5 A, B). CYT387 led to a reduction in the mRNA and protein levels of c-Fos in CPM resistant cell lines (Figure 5 C). Although CYT387 treatment did not lead to robust cell death, it profoundly decreased cell density (Supplementary Figure 5 C). BRDU incorporation and cell cycle analysis indicated a significant (> 50%) reduction in cell proliferation at 3 μ M CYT387 in Th-*MYCN*^{CPM32} cell lines but not in KELLY cells (Figure 5 D). Following pre-treatment with CYT387 in IMR5 and 96459B, both showed a reduction in colony formation with or without continued CYT387 treatment (Figure 5 E). To confirm that the effect of CYT387 is related to the inhibition of STAT3, we genetically manipulated STAT3 levels using an siRNA and a STAT3 overexpression vector. Abrogation of STAT3 phenocopied the effect of CYT387 treatment, causing a 25% reduction in cell proliferation as compared to transfection with a non-targeted control siRNA (Supplementary Figure 6 A, B). Re-expression of STAT3 partially rescued cells following CYT387 treatment, and increased cell viability from 49% \pm 1.575% in control cells to 61% \pm 2.24% in STAT3 overexpression cells (supplementary Figure 6 C, D).

To test whether CYT387 is effective in the setting of chemoresistance and upregulation of STAT3 signaling, we used Th-*MYCN*^{CPM32} cell lines, which are relatively resistant to 4-hydroperoxy Cyclophosphamide (4-OOH-CY), vincristine and doxorubicin, as compared to the human *MYCN*-amplified neuroblastoma sensitive cell line IMR5, (Supplementary Figure 6 E, F, G). In all three Th-*MYCN*^{CPM32} cell lines, addition of CYT387 partially restored sensitivity to 4-OOH-CY (Figure 5 F, G) and vincristine (Figure 5 H, I) as measured by area under the curve (AUC) reduction. These results suggest that CYT387 may have therapeutic potential in chemoresistant neuroblastoma.

*In vivo treatment with CYT387 reduces tumor growth and increases survival in Th-*MYCN*^{CPM32} allografts*

In order to more precisely establish the *in vivo* efficacy of CYT387 in a treatment resistant setting, we used subcutaneous allografts of cells excised from Th-*MYCN* or Th-*MYCN*^{CPM32} tumors in 129X1/SvJ (immunocompetent, strain-matched) mice. As expected, Th-*MYCN*^{CPM32} allografts were refractory to CPM treatment with a 160% mean growth at 7 days after treatment (Figure 6 A), while Th-*MYCN* allografts underwent complete regression at a dose of 32 mg/kg CPM. In contrast, treatment with 32 mg/kg CPM (once per week) together with 50 mg/kg CYT387 (administered 5 days on 2 days off) significantly reduced tumor volume at day 5 in the treatment resistant Th-*MYCN*^{CPM32} allograft tumors from a mean of 152% ± 21% to 82% ± 20% (Figure 6 B). Furthermore, we observed an increase in survival of 6 days (representing of 37%) from a median of 16 days to a median of 22 days. These results establish that the acquisition of chemoresistance following treatment with CPM is transplantable, therefore cell-intrinsic, and that *in vivo* treatment with the JAK STAT inhibitor CYT387 reduces tumor growth and extends survival in CPM chemoresistant neuroblastoma.

DISCUSSION

There is a clear need to develop novel therapeutic strategies for children with high-risk neuroblastoma who become resistant to conventional treatment. The difficulty of obtaining surgical biopsies at time of relapse, and the lack of model systems that faithfully recapitulate chemoresistant neuroblastoma together with clinically relevant distant metastases has hindered further mechanistic understanding of the biology that underpins the emergence of chemoresistant, metastatic disease.

We have optimized the well-established Th-*MYCN* transgenic model of neuroblastoma, which develops many features of aggressive neuroblastoma but lacks distant metastases. We report that Th-*MYCN* tumors acquire cell-intrinsic resistance to cyclophosphamide (CPM) and cross-resistance to other chemotherapeutics following prolonged genotoxic treatment with CPM alone. Concurrently, the majority of mice develop metastases to bone marrow, gain of the chromosomal region equivalent to the human 17q and expression of 17q- equivalent localized genes. Furthermore, resistant tumors present microenvironmental-stromal changes and mesenchymal markers suggestive of transition to a migratory-invasive and mesenchymal phenotype. Taken

together, these features suggest a model of chemorefractory neuroblastoma that has many of the hallmarks of high-risk chemoresistant metastatic disease.

Tumor-stromal interactions and ECM alterations, together with development of an EMT pro-migratory signature, play a role in drug resistance and in the development of a metastatic phenotype (24,35,36). We demonstrated an increase in collagen IV content and bundle thickness in the chemoresistant model of neuroblastoma (Th-*MYCN*^{CPM32}), consistent with similar observations in lung cancer cells, where increased collagen IV deposition stimulates integrin β 1 - PI3K pathway activity, and supports a pro-survival, drug resistant state (37). In neuroblastoma, analysis of 102 primary high-risk tumors demonstrated large reticulin fiber networks (19). Taking this data into account, we suggest that the alterations in ECM we observe in this experimental model of chemoresistant neuroblastoma are likely to be associated with development of resistance, although further work will be required to establish the mechanism for this association.

An alternative possibility is that alterations in tumor-stromal interactions and changes in ECM structure can directly impair drug efficacy by acting as a physical barrier to drug penetration (38). In this model, pharmacokinetic studies did not detect any significant changes in intratumoral drug levels of cyclophosphamide or its metabolites in resistant compared with treatment naive tumours. This, together with the observation that cells removed from resistant Th-*MYCN*^{CPM32} tumors maintained resistance to cyclophosphamide and acquired cross-resistance to additional drugs in derivative cell-culture, suggests that development of chemoresistance in this model is cell-intrinsic.

Consistent with prior reports, the development of chemoresistance in the Th-*MYCN*^{CPM32} model may be linked with transition toward a mesenchymal state. In neuroblastoma, expression of genes associated with the mesenchymal core-regulatory state correlates with enhanced *in vitro* resistance to standard neuroblastoma chemotherapy drugs such as cisplatin, doxorubicin, and etoposide, and is thought to be one feature associated with development of aggressive disease (9). We detected a proportion of cells in Th-*MYCN*^{CPM32} resistant tumors that exhibit changes in genes and protein expression, consistent with transition toward a mesenchymal state. In keeping with this, bulk RNAseq of Th-*MYCN*^{CPM32} and Th-*MYCN* tumor specimens only demonstrated a non-significant trend towards the mesenchymal phenotype in the Th-*MYCN*^{CPM32}. However, in Th-*MYCN*^{CPM32} derived *ex vivo* culture we observe a more distinct mesenchymal signature. This may be a consequence of expansion of these cells related to a preferential cell-culture

microenvironment or alternatively enhanced growth properties that are intrinsic to mesenchymal cells. Further mechanistic studies will shed light on these observations. The reduction in MYCN levels seen in our Th-MYCN^{CPM32} derived cell lines may also be associated with their mesenchymal type; it has previously been reported that MYCN amplified lines are consistently adrenergic, whereas cell lines without MYCN amplification may display either signature (39).

Tumors from mice with refractory and metastatic disease were characterized by genomic changes and altered expression patterns characteristic of aggressive disease in human patients; gain of a chromosomal region syntenic to human 17q, *Ccnb1p1* and *TK1* upregulation, and alterations in the JAK-STAT3 pathway. In contrast to neuroblastoma, upregulation of *Ccnb1p1*, an ubiquitin ligase, in lung and breast cancer is correlated with prolonged survival (40). Although some of the known molecular functions of CCNB1IP1 would support a tumor suppressor role, its mechanism of action and its full interactive network is not yet completely characterized. TK1 levels are a diagnostic marker useful for clinical decision making in treatment of several malignancies, such as pediatric acute lymphoblastic leukemia (25,41).

The JAK-STAT3 pathway is upregulated in aggressive neuroblastoma and in the Th-MYCN^{CPM32} mice. In previously published *in vivo* models of neuroblastoma, Withaferin A, a non-exclusive STAT3 inhibitor, and AZD1480, a JAK1/2 inhibitor, both increase tumor cell death through induction of apoptosis (42,43). We find that the clinical candidate JAK1/JAK2 inhibitor CYT387 counteracts *in vitro* resistance to both the CPM active metabolite 4-OOH-CY and to vincristine. Furthermore, *in vivo* combination with CPM leads to substantial growth arrest of these highly aggressive chemorefractory tumors, resulting in an increase in overall survival. In neuroblastoma xenografts, STAT3 modulates drug response through activation of the pro-survival, anti-apoptotic protein Bcl-xL, and increases metastatic potential (44). The JAK-STAT3 pathway is a major regulator of tumor-cell invasion and immunomodulatory pathways that are co-opted by tumorigenesis (45), implying a complex interaction between tumor cells and the microenvironment. We therefore cannot exclude that the increased signature of the JAK-STAT3 pathway, and the *in vivo* therapeutic benefit of CYT387 in our model, might arise both from the tumor cells and/or from the tumor microenvironment.

To summarize, we have generated a model of neuroblastoma that spontaneously recapitulates the chemoresistance and bone-marrow metastases typical of neuroblastoma patients at relapse. In the context of genotoxic stress resembling clinical therapy, we observe concomitant

evidence of genomic and microenvironmental alterations consistent with development of high-risk, metastatic neuroblastoma in patients. The emergence of mesenchymal-like cells within these tumors, that are a potential source for the metastases that we observe, is an intriguing finding for further study. Finally, this fully immunocompetent, chemorefractory and metastatic tumor model of aggressive, relapsed/refractory neuroblastoma provides an essential tool for further development of targeted treatment approaches, such as the suggested STAT3 inhibition, in a clinically relevant context.

Acknowledgments: We would like to thank Gary Box for assisting with *in vivo* work and Igor Vivanco and Evon Poon for critical reading of the manuscript.

Data and materials availability: We would like to thank Professor Clare Isacke and Dr Ute Jungwirth for providing ECM antibodies and advice and Dyanne Rampling for assisting in obtaining the human neuroblastoma images.

REFERENCES

1. Maris JM, Hogarty MD, Bagatell R, Cohn SL. Neuroblastoma. *Lancet* **2007**;369:2106-20
2. Garaventa A, Parodi S, De Bernardi B, Dau D, Manzitti C, Conte M, *et al.* Outcome of children with neuroblastoma after progression or relapse. A retrospective study of the Italian neuroblastoma registry. *European journal of cancer* **2009**;45:2835-42
3. Dalzell AM, Mistry P, Wright J, Williams FM, Brown CD. Characterization of multidrug transporter-mediated efflux of avermectins in human and mouse neuroblastoma cell lines. *Toxicology letters* **2015**;235:189-98
4. Middlemas DS, Stewart CF, Kirstein MN, Poquette C, Friedman HS, Houghton PJ, *et al.* Biochemical correlates of temozolomide sensitivity in pediatric solid tumor xenograft models. *Clinical cancer research : an official journal of the American Association for Cancer Research* **2000**;6:998-1007
5. Schleiermacher G, Javanmardi N, Bernard V, Leroy Q, Cappo J, Rio Frio T, *et al.* Emergence of new ALK mutations at relapse of neuroblastoma. *Journal of clinical oncology : official journal of the American Society of Clinical Oncology* **2014**;32:2727-34
6. Schramm A, Koster J, Assenov Y, Althoff K, Peifer M, Mahlow E, *et al.* Mutational dynamics between primary and relapse neuroblastomas. *Nature genetics* **2015**;47:872-7
7. Eleveld TF, Oldridge DA, Bernard V, Koster J, Colmet Daage L, Diskin SJ, *et al.* Relapsed neuroblastomas show frequent RAS-MAPK pathway mutations. *Nature genetics* **2015**;47:864-71
8. Boeva V, Louis-Brennetot C, Peltier A, Durand S, Pierre-Eugene C, Raynal V, *et al.* Heterogeneity of neuroblastoma cell identity defined by transcriptional circuitries. *Nature genetics* **2017**;49:1408-13
9. van Groningen T, Koster J, Valentijn LJ, Zwijnenburg DA, Akogul N, Hasselt NE, *et al.* Neuroblastoma is composed of two super-enhancer-associated differentiation states. *Nature genetics* **2017**;49:1261-6
10. Chesler L, Weiss WA. Genetically engineered murine models--contribution to our understanding of the genetics, molecular pathology and therapeutic targeting of neuroblastoma. *Semin Cancer Biol* **2011**;21:245-55
11. Weiss WA, Aldape K, Mohapatra G, Feuerstein BG, Bishop JM. Targeted expression of MYCN causes neuroblastoma in transgenic mice. *The EMBO journal* **1997**;16:2985-95
12. Zhao F, He X, Wang Y, Shi F, Wu D, Pan M, *et al.* Decrease of ZEB1 expression inhibits the B16F10 cancer stem-like properties. *Bioscience trends* **2015**;9:325-34
13. Egler RA, Burlingame SM, Nuchtern JG, Russell HV. Interleukin-6 and soluble interleukin-6 receptor levels as markers of disease extent and prognosis in neuroblastoma. *Clinical cancer research : an official journal of the American Association for Cancer Research* **2008**;14:7028-34
14. Workman P, Aboagye EO, Balkwill F, Balmain A, Bruder G, Chaplin DJ, *et al.* Guidelines for the welfare and use of animals in cancer research. *British journal of cancer* **2010**;102:1555-77
15. McGrath JC, Drummond GB, McLachlan EM, Kilkenny C, Wainwright CL. Guidelines for reporting experiments involving animals: the ARRIVE guidelines. *Br J Pharmacol* **2010**;160:1573-6
16. Yogev O, Barker K, Sikka A, Almeida GS, Hallsworth A, Smith LM, *et al.* p53 Loss in MYC-Driven Neuroblastoma Leads to Metabolic Adaptations Supporting Radioresistance. *Cancer research* **2016**;76:3025-35
17. Yoshida A, Dave V, Han H, Scanlon KJ. Enhanced transcription of the cytosolic ALDH gene in cyclophosphamide resistant human carcinoma cells. *Adv Exp Med Biol* **1993**;328:63-72
18. Chinnaswamy G, Errington J, Foot A, Boddy AV, Veal GJ, Cole M. Pharmacokinetics of cyclophosphamide and its metabolites in paediatric patients receiving high-dose myeloablative therapy. *European journal of cancer* **2011**;47:1556-63
19. Tadeo I, Berbegall AP, Castel V, Garcia-Miguel P, Callaghan R, Pahlman S, *et al.* Extracellular matrix composition defines an ultra-high-risk group of neuroblastoma within the high-risk patient cohort. *British journal of cancer* **2016**;115:480-9
20. Debruyne DN, Bhatnagar N, Sharma B, Luther W, Moore NF, Cheung NK, *et al.* ALK inhibitor resistance in ALK(F1174L)-driven neuroblastoma is associated with AXL activation and induction of EMT. *Oncogene* **2016**;35:3681-91
21. Piskareva O, Harvey H, Nolan J, Conlon R, Alcock L, Buckley P, *et al.* The development of cisplatin resistance in neuroblastoma is accompanied by epithelial to mesenchymal transition in vitro. *Cancer letters* **2015**;364:142-55

22. Nozato M, Kaneko S, Nakagawara A, Komuro H. Epithelial-mesenchymal transition-related gene expression as a new prognostic marker for neuroblastoma. *International journal of oncology* **2013**;42:134-40
23. Tsai JH, Donaher JL, Murphy DA, Chau S, Yang J. Spatiotemporal regulation of epithelial-mesenchymal transition is essential for squamous cell carcinoma metastasis. *Cancer Cell* **2012**;22:725-36
24. Vu T, Datta PK. Regulation of EMT in Colorectal Cancer: A Culprit in Metastasis. *Cancers (Basel)* **2017**;9
25. Zhou J, He E, Skog S. The proliferation marker thymidine kinase 1 in clinical use. *Molecular and clinical oncology* **2013**;1:18-28
26. Jagarlamudi KK, Shaw M. Thymidine kinase 1 as a tumor biomarker: technical advances offer new potential to an old biomarker. *Biomark Med* **2018**;12:1035-48
27. Bown N, Lastowska M, Cotterill S, O'Neill S, Ellershaw C, Roberts P, *et al.* 17q gain in neuroblastoma predicts adverse clinical outcome. U.K. Cancer Cytogenetics Group and the U.K. Children's Cancer Study Group. *Med Pediatr Oncol* **2001**;36:14-9
28. Pugh TJ, Morozova O, Attiyeh EF, Asgharzadeh S, Wei JS, Auclair D, *et al.* The genetic landscape of high-risk neuroblastoma. *Nature genetics* **2013**;45:279-84
29. Ara T, Song L, Shimada H, Keshelava N, Russell HV, Metelitsa LS, *et al.* Interleukin-6 in the bone marrow microenvironment promotes the growth and survival of neuroblastoma cells. *Cancer research* **2009**;69:329-37
30. Keshelava N, Seeger RC, Groshen S, Reynolds CP. Drug resistance patterns of human neuroblastoma cell lines derived from patients at different phases of therapy. *Cancer Res* **1998**;58:5396-405
31. Thiele CJ. Neuroblastoma Cell Lines. **1998**;Vol 1,: p 21-53
32. Morrison LJ, Cochran AJ, Gibson AA, Willoughby ML, More IA. Establishment and characterization of human neuroblastoma and ganglioneuroblastoma cell lines. *British journal of cancer* **1982**;45:531-42
33. Tumilowicz JJ, Nichols WW, Cholon JJ, Greene AE. Definition of a continuous human cell line derived from neuroblastoma. *Cancer research* **1970**;30:2110-8
34. Snyder M, Huang XY, Zhang JJ. Identification of novel direct Stat3 target genes for control of growth and differentiation. *The Journal of biological chemistry* **2008**;283:3791-8
35. Du B, Shim JS. Targeting Epithelial-Mesenchymal Transition (EMT) to Overcome Drug Resistance in Cancer. *Molecules* **2016**;21
36. Kumar S, Das A, Sen S. Extracellular matrix density promotes EMT by weakening cell-cell adhesions. *Molecular bioSystems* **2014**;10:838-50
37. Su C, Su B, Tang L, Zhao Y, Zhou C. Effects of collagen iv on cisplatin-induced apoptosis of non-small cell lung cancer cells. *Cancer investigation* **2007**;25:542-9
38. Tannock IF, Lee CM, Tunggul JK, Cowan DS, Egorin MJ. Limited penetration of anticancer drugs through tumor tissue: a potential cause of resistance of solid tumors to chemotherapy. *Clinical cancer research : an official journal of the American Association for Cancer Research* **2002**;8:878-84
39. Durbin AD, Zimmerman MW, Dharia NV, Abraham BJ, Iniguez AB, Weichert-Leahey N, *et al.* Selective gene dependencies in MYCN-amplified neuroblastoma include the core transcriptional regulatory circuitry. *Nature genetics* **2018**;50:1240-6
40. Confalonieri S, Quarto M, Goisis G, Nuciforo P, Donzelli M, Jodice G, *et al.* Alterations of ubiquitin ligases in human cancer and their association with the natural history of the tumor. *Oncogene* **2009**;28:2959-68
41. Hagag AA, Saad MA, Mohamed SA. Clinical significance of thymidine kinase in Egyptian children with acute lymphoblastic leukemia. *South Asian journal of cancer* **2015**;4:72-4
42. Yco LP, Mocz G, Opoku-Ansah J, Bachmann AS. Withaferin A Inhibits STAT3 and Induces Tumor Cell Death in Neuroblastoma and Multiple Myeloma. *Biochemistry insights* **2014**;7:1-13
43. Yan S, Li Z, Thiele CJ. Inhibition of STAT3 with orally active JAK inhibitor, AZD1480, decreases tumor growth in Neuroblastoma and Pediatric Sarcomas In vitro and In vivo. *Oncotarget* **2013**;4:433-45
44. Ara T, Nakata R, Sheard MA, Shimada H, Buettner R, Groshen SG, *et al.* Critical role of STAT3 in IL-6-mediated drug resistance in human neuroblastoma. *Cancer research* **2013**;73:3852-64
45. Yu H, Lee H, Herrmann A, Buettner R, Jove R. Revisiting STAT3 signalling in cancer: new and unexpected biological functions. *Nature reviews Cancer* **2014**;14:736-46

Table 1. – Individualized multicycle CPM treatment of Th-MYCN tumor bearing mice

Sample number	# cycles at 16 mg/kg	# cycles at 24 mg/kg	# cycles at 32 mg/kg	# CPM cycles	Duration of trial (days)	p-STAT3 (Y705) staining (*)	Metastases (1,*)	Imaging
Res 1 (54001)	1	1	8	10	81	N/A	N/A	
Res 2 (53510)	2	1	2	5	64	N/A	N/A	
Res 3 (69078)	3	5	3	11	64	-	N/A	
Res 4 (57507)	5	1	7	13	75	-	N/A	
Res 5 (104453)	7	3	2	12	97	N/A	N/A	
Res 6 (77709)	2	1	3	6	34	√	√	
Res 7 (88793)	3	4	2	9	58	√	√	√
Res 8 (88790)	3	5	3	11	68	√	√	√
Res 9 (104468)	3	5	3	11	63	√	√	
Res 10 (68557)	5	7	2	14	81	√	√	
Res 11 (108809)	4	5	2	11	66	-	√	√
Res 12 (108807)	3	3	2	8	46	√	√	√
Res 13 (108832)	9	1	8	18	116	-	√	√
Res 14 (104457)	4	2	5	11	94	N/A	√	
Res 15 (108851)	6	4	2	12	80	-	-	√
Res 16 (107389)	8	2	6	16	120	-	-	√
Res 17 (105895)	3	3	4	10	74	√	-	√
Res 18 (110232)	2	1	3	6	71	-	-	√
Average	4	3	4	11	75			
Stdev	2	2	2	3	22			
SEM	1	0	1	1	5			

Table 1 - Summary of Th-MYCN mice subject to the individual dose escalation protocol.

1. Metastasis was confirmed in n = 9/13 by IHC for the mouse neuroblastoma marker NF-L. Positive sections range from single cells to cell clusters and larger focal metastases.

* N/A - sample unavailable

Table 2. GSEA for KEGG pathways

NAME	FDR.q.val*
KEGG_PPAR_SIGNALING_PATHWAY	0
KEGG_PROXIMAL_TUBULE_BICARBONATE_RECLAMATION	0.000652174
KEGG_TERPENOID_BACKBONE_BIOSYNTHESIS	0.025131369
KEGG_SYSTEMIC_LUPUS_ERYTHEMATOSUS	0.003503739
KEGG_LEISHMANIA_INFECTION	0.002657667
KEGG_TYPE_I_DIABETES_MELLITUS	0.003315611
KEGG_LYSOSOME	0.00430583
KEGG_CYTOKINE_CYTOKINE_RECEPTOR_INTERACTION	0.004022749
KEGG_JAK_STAT_SIGNALING_PATHWAY	0.007673774
KEGG_HEMATOPOIETIC_CELL_LINEAGE	0.011372167
KEGG_ASTHMA	0.013715881
KEGG_B_CELL_RECEPTOR_SIGNALING_PATHWAY	0.01668986
KEGG_AUTOIMMUNE_THYROID_DISEASE	0.020905254
KEGG_CYTOSOLIC_DNA_SENSING_PATHWAY	0.022730485
KEGG_HISTIDINE_METABOLISM	0.022762213

Table 2- Significantly enriched KEGG pathways based on fold-changes of gene expression between Th-MYCN^{CPM32} and Th-MYCN.

The gene set enrichment analysis (GSEA) was performed with the MSigDB gene collections. 15 out of 186 KEGG pathways were found to be statistically significant.

*FDR (False Discovery Rate), adjusted p-value (Benjamini Hochberg method).

Figure 1

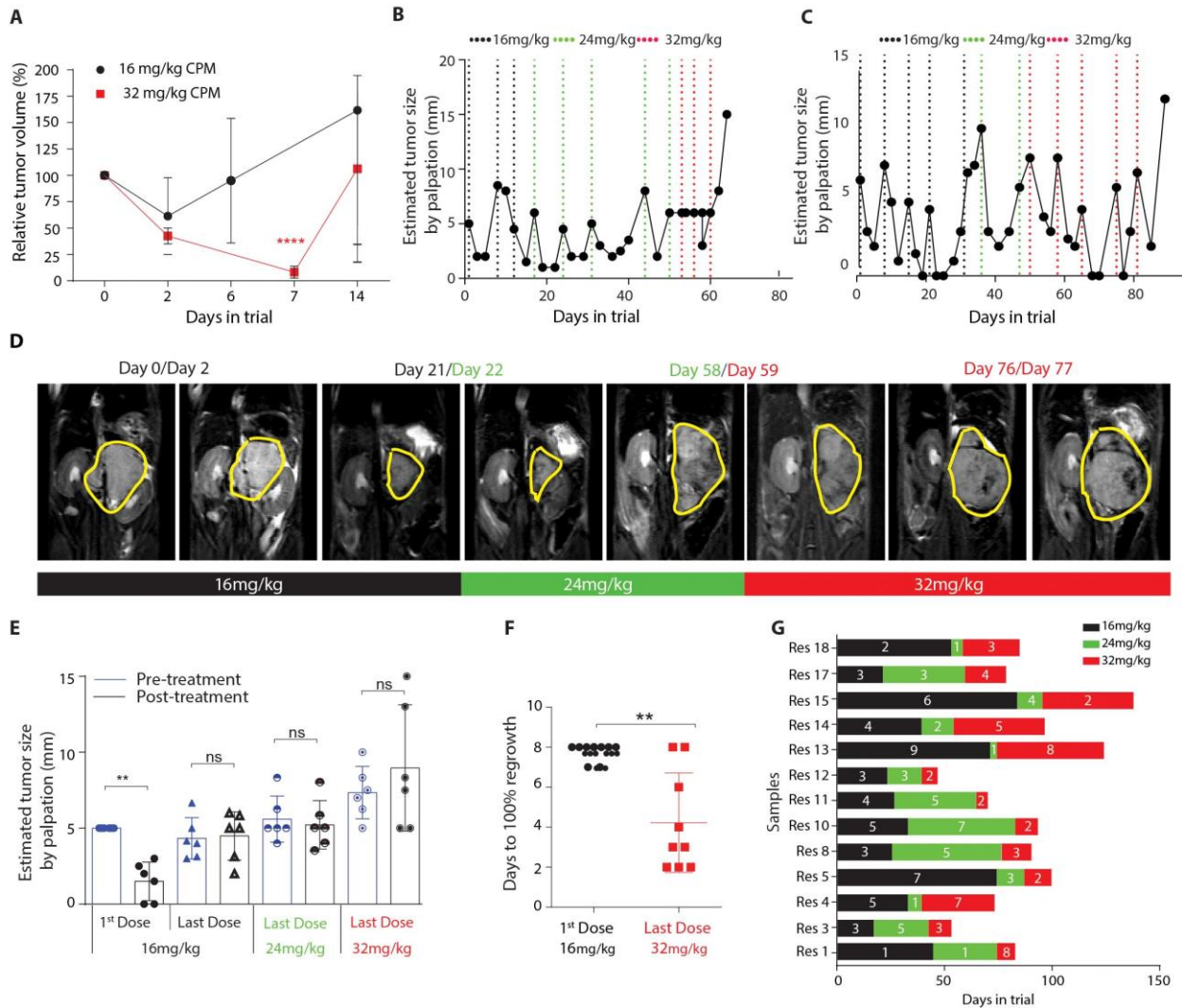


Figure 1. Personal dose escalation leads to acquired resistance to CPM in Th-MYCN mice.

(A) Changes in tumor volume measured by MRI (% of baseline) after a single dose of 16 mg/kg ($n = 4$) or 32 mg/kg CPM ($n = 12$), **** P -value < 0.001 unpaired t test. (B) & (C) Representative longitudinal tumor response for 2 individual mice over the course of the personal dose escalation (PDE). Dotted lines represent the time of dosing at 16 mg/kg (black), 24 mg/kg (green) and 32 mg/kg (red). (D) Representative presentation of 2D image of T₂-weighted MRI schedule, before and after each dose escalation (tumors delineated in yellow). (E) Estimated tumor size by palpation during the multicycle dose escalation protocol. Graph shows tumor size pre-treatment and 4 days post-treatment for the initial dosing (16 mg/kg) and the last dosing for each stage of acquired

resistance (16 mg/kg, 24 mg/kg, 32 mg/kg), $n = 6$, $**P - \text{value} = 0.0011$; paired t test. **(F)** Time (days) to regrowth following the first treatment of 16 mg/kg and the last treatment of 32 mg/kg, $** P - \text{value} = 0.0031$ paired t test **(G)** Summary of individualized dose escalation treatment schedule (numbers represent the amount of single doses).

Figure 2

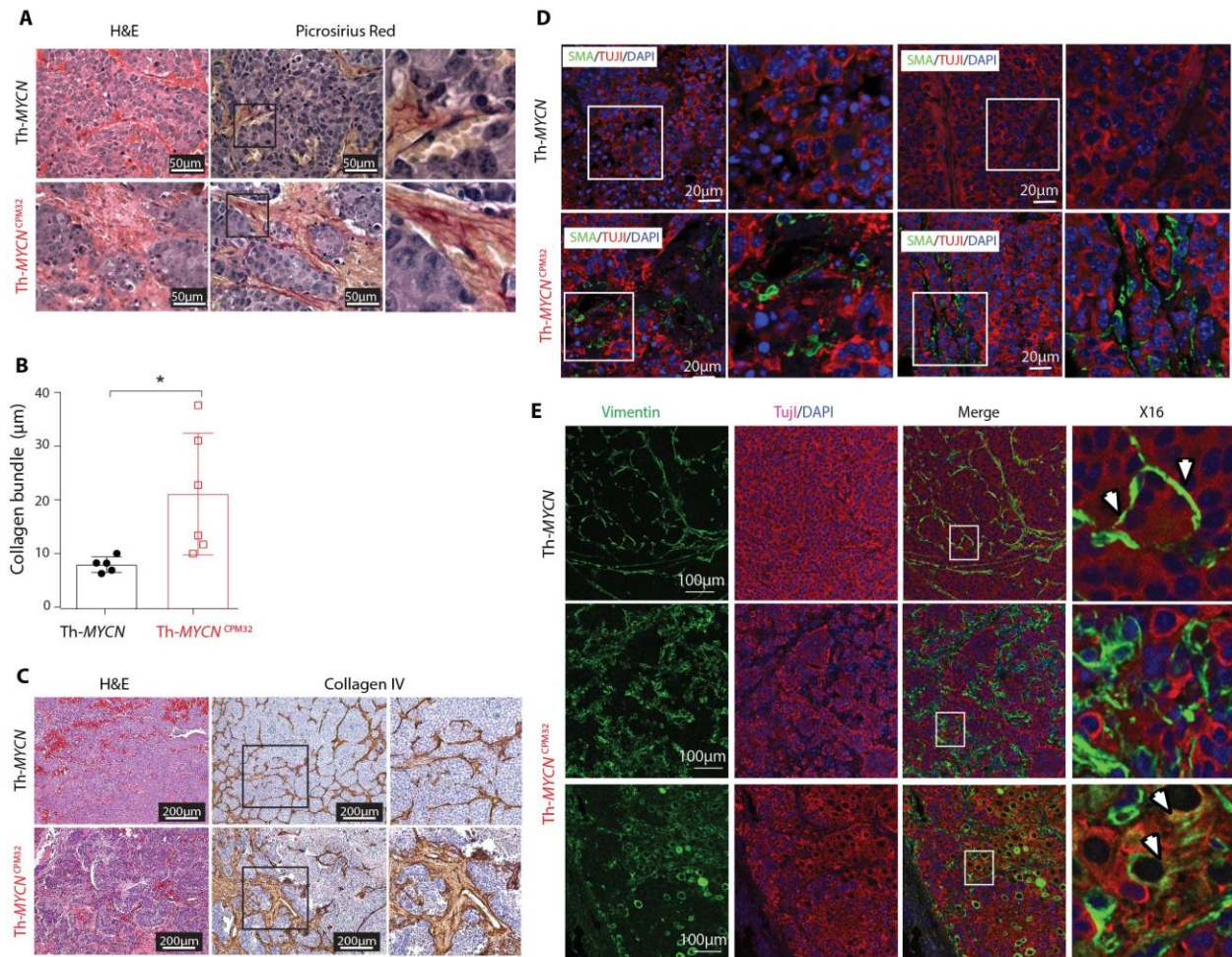


Figure 2. Resistant tumors show enhanced ECM.

(A) Representative images of tumor sections from Th-MYCN and Th-MYCN^{CPM32} stained with Picrosirius Red for total collagen (red). Cell nuclei were counterstained with hematoxylin. Scale bar: 50μm. (B) Collagen bundle width (μm) for Th-MYCN ($n = 5$) and Th-MYCN^{CPM32} ($n = 6$), mean SEM, * P - value = 0.0313, unpaired t test. (C) Representative images of tumor sections from Th-MYCN and Th-MYCN^{CPM32} stained for Collagen IV (brown). Cell nuclei were counterstained with hematoxylin. Scale bar: 200 μm. (D) Representative images of tumor sections from Th-MYCN and Th-MYCN^{CPM32} stained for tumor associated fibroblasts (smooth muscle actin: SMA) (green), neural marker (β -tubulin III: TujI) (red) and DAPI (blue). Scale bar: 20 μm. (E) Representative images of tumor sections from Th-MYCN and Th-MYCN^{CPM32} stained for vimentin

(green), Tuji (red) and DAPI (blue). Arrows indicating vimentin positive endothelial-like cells, top image, and vimentin Tuji co-stained tumor cells, lower image. Scale bar: 100 μm .

Figure 3

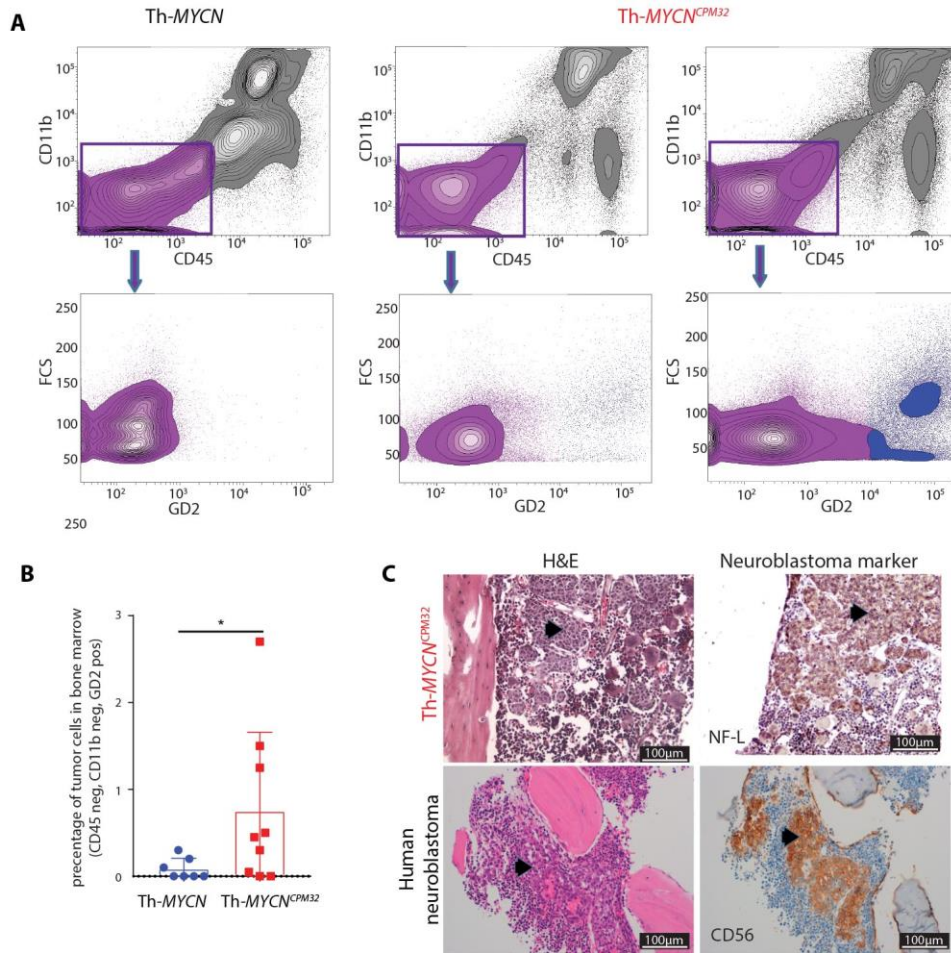


Figure 3. Resistant tumors show enhanced bone marrow metastatic disease.

(A) Representative gating strategy of metastatic cells in the bone marrow. Single live cells negative for CD45 and CD11b (purple cells) were plotted for their GD2 levels (GD2 high cells shown in blue). (B) Percentage of tumor cells in the bone marrow from Th-MYCN (n = 7) and Th-MYCN^{CPM32} (n = 9), mean SEM, * P - value = 0.038 one way t test, (C) Top Panel - Representative images of tibia sections from Th-MYCN^{CPM32} subjected to H&E and immunohistochemical staining for the mouse neuroblastoma marker neurofilament-light (NF-L). Cell nuclei were counterstained with hematoxylin. Scale bar: 100 μ m. Lower Panel - Human neuroblastoma trephine subjected to H&E and immuno-histochemical staining for the neuroblastoma human marker CD56, and counterstained with hematoxylin . Black arrows indicate bone marrow metastases.

Figure 4

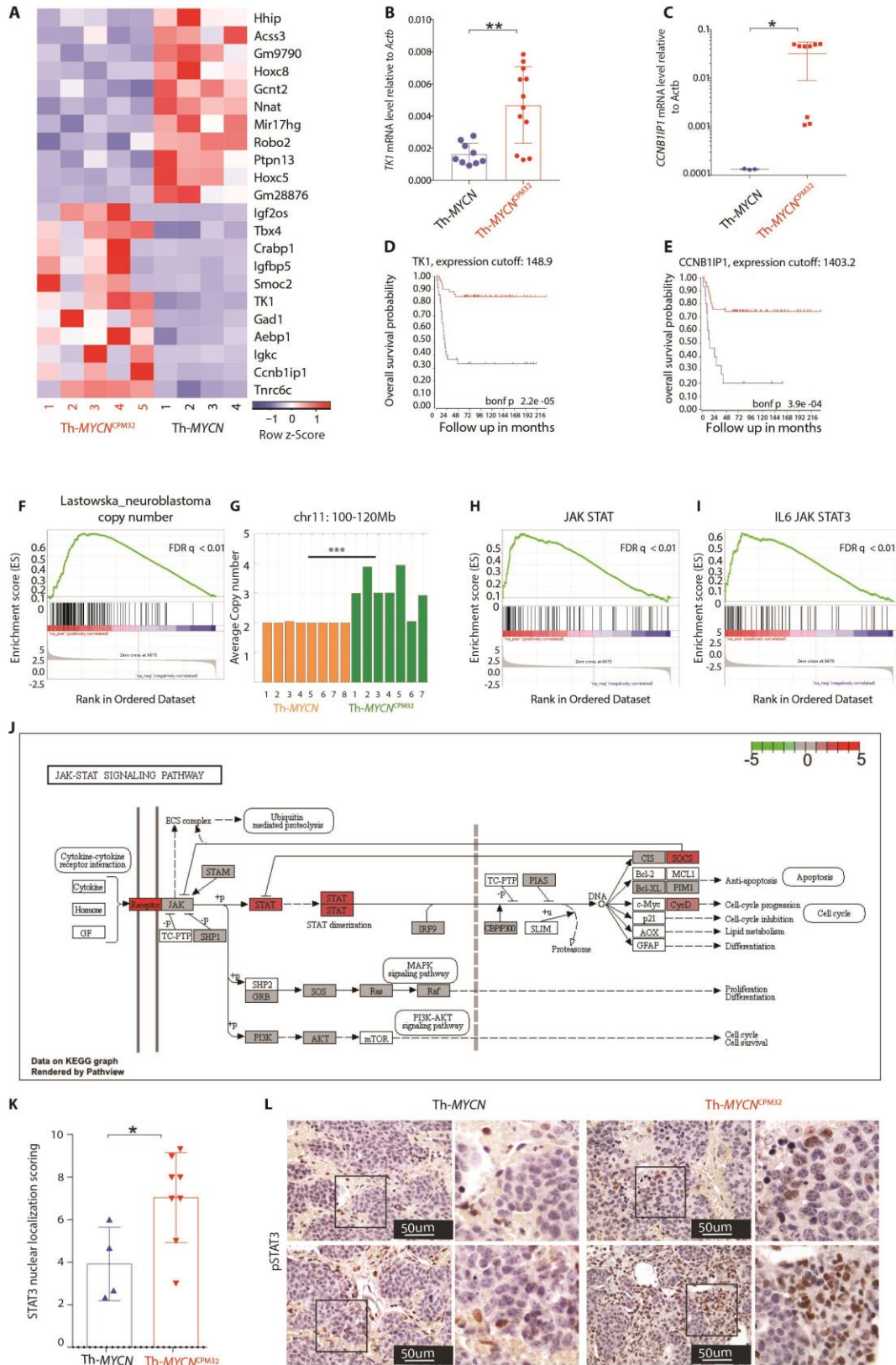


Figure 4. Resistant tumors show upregulation of genes associated with neuroblastoma poor survival and JAK STAT pathway activation.

(A) Heatmap of RNA sequence analysis of Th-*MYCN* ($n = 4$) and Th-*MYCN*^{CPM32} ($n = 5$) tumors. (B-C) RT-PCR analysis of *TK1* and *Ccnblip1* mRNA expression relative to *Actb*, dots represent tumors with detectable value, ** P - value = 0.0015, * P - value = 0.0435 unpaired t test. (D-E) Overall survival of human neuroblastoma patients according to low (red) or high (blue) expression of *TK1* and *Ccnblip1* (<http://r2.amc.nl>, Versteeg-88 database of human neuroblastoma samples, GEO Series GSE16476). (F) Graphic representation of gene set enrichment analysis (GSEA) for LASTOWSKA NEUROBLASTOMA COPY NUMBER UP. (G) Copy number analysis of whole exome sequencing for murine chromosome 11 region 100-120Mb, *** P - value = 0.003, Wilcoxon rank sum test. (H-I) Graphic representation of gene set enrichment analysis (GSEA) for KEGG JAK STAT SIGNALING PATHWAY and IL6 JAK STAT3, FDR $q < 0.01$. (J) Schematic diagram of the KEGG JAK/STAT pathway, upregulated genes in Th-*MYCN*^{CPM32} tumors are marked in red (K) STAT3 nuclear localization scoring based on STAT3 immunohistochemistry * P - value = 0.0157, unpaired t test. (L) Representative images of tumor sections from Th-*MYCN* and Th-*MYCN*^{CPM32} stained for pSTAT3 Y705 (brown); cell nuclei were counterstained with hematoxylin. Scale bar: 50 μ m.

Figure 5

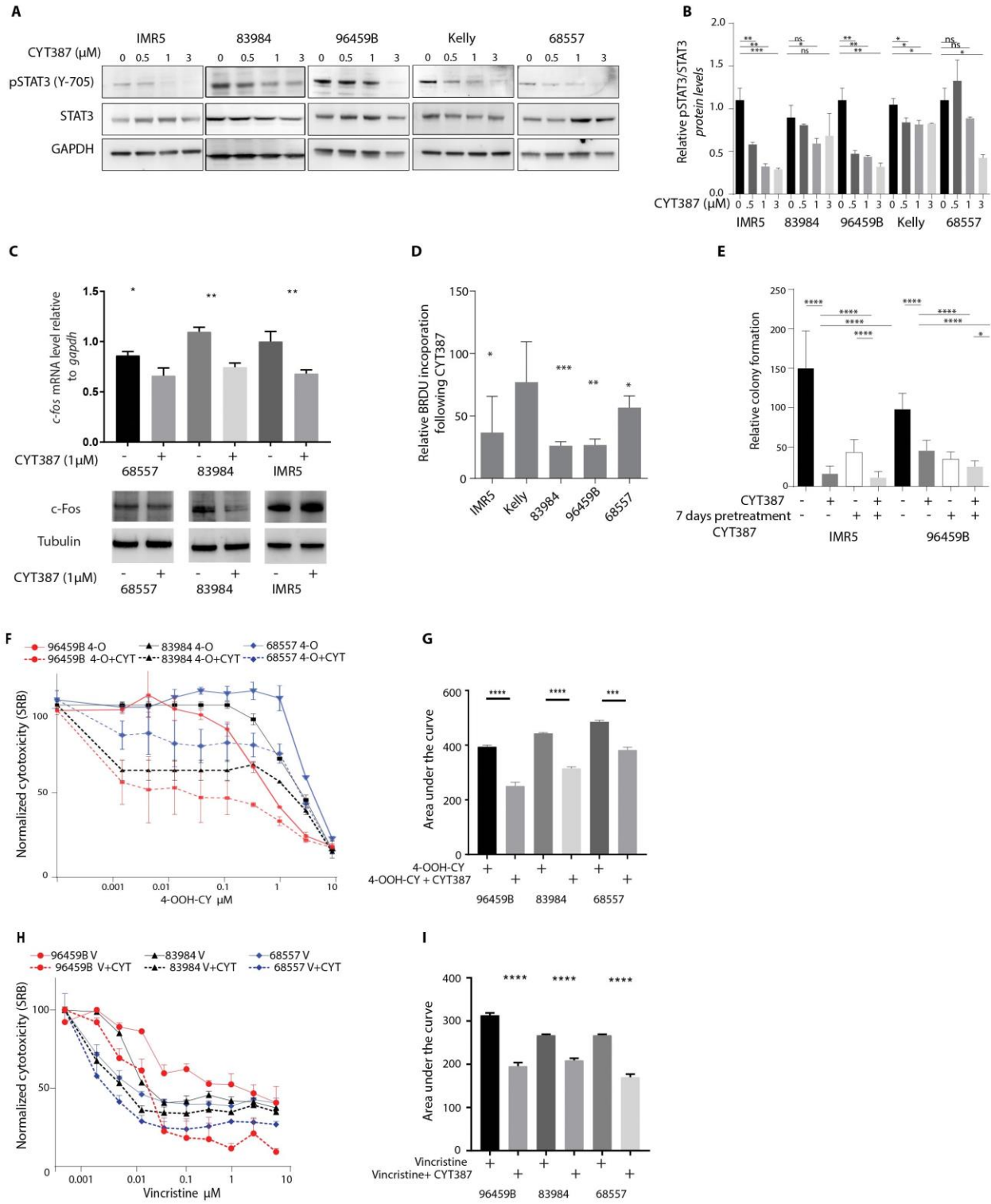


Figure 5. Th-MYC^{CPM32} derived cell lines retain multi-drug resistance and are sensitive to CYT387.

(A) Immunoblot for p-STAT3, STAT3 and GAPDH levels at 24h post treatment with CYT387. (B) Relative pSTAT3/STAT3 expression (Dunnett's multiple comparisons test one way Anova). (C) Top panel - RT-PCR analysis of *c-fos* mRNA expression relative to *GAPDH*; lower panel - immunoblot for c-Fos protein levels. * *P* - value = 0.0289, ** *P* - value = 0.0025, **** *P* - value = < 0.0001 unpaired t test (*n* = 3). (D) Mean of BRDU incorporation following CYT387 treatment (3 independent experiments), * *P* - value = 0.0454, *** *P* - value = 0.0005, ** *P* - value = 0.0010, * *P* - value = 0.0114. (E) Colony formation assay of CYT387 pretreated and control cells with and without the drug, **** *P* - value = < 0.0001; * *P* - value = 0.0288 unpaired t test, (*n* = 6 in 2 independent experiments). (F) SRB cytotoxicity assay; 4-hydroperoxy cyclophosphamide (4-OOH-CY) (solid line) or 4-OOH-CY and 1 μM CYT387 (dashed line) (*n* = 6 in 2 independent experiments). (G) Area under the curve reflects both the sensitivity and the toxicity of the drug. **** *P* - value < 0.0001, *** *P* - value = 0.0001, paired t test. (H) SRB cytotoxicity assay; vincristine (solid line) or vincristine and 1 μM CYT387 (dashed line) (*n* = 6 in 2 independent experiments). (I) Area under the curve reflects both the sensitivity and the toxicity of the drug. **** *P* - value < 0.0001, paired t test.

Fig 6.

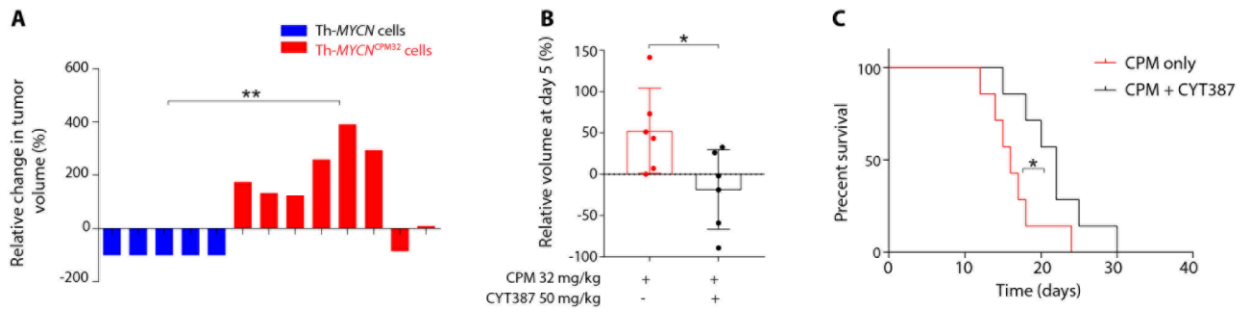


Figure 6. *In vivo* treatment with CYT387 reduced tumor growth and enhanced survival.

(A) Relative tumor size at day 7 after 40 mg/kg CPM treatment of allografts from Th-MYCN ($n = 5$) and Th-MYCN^{CPM32} ($n = 8$) primary cells. ** P - value = 0.0032. (B) Relative tumor size of allografts from Th-MYCN^{CPM32} ($n = 6$) primary cells at day 5 post 32 mg/kg CPM, with or without 50 mg/kg CYT387 treatment. * P - value = 0.0164 unpaired t test. (C) Kaplan-Meier Tumor free survival curves for allografts from Th-MYCN^{CPM32} treated with 32 mg/kg CPM and with or without 50 mg/kg CYT387 ($n = 7$) * P - value = 0.044 Log-rank (Mantel-Cox) test.